Mining, Metallurgy & Exploration
https://doi.org/10.1007/s42461-024-01072-5

Prediction of Backbreak in Surface Production Blasting Using 3-Dimensional Finite Element Modeling and 3-Dimensional Nearfield Vibration Modeling

Satyabrata Behera[1] · **Kaushik Dey**[2]

Received: 2 April 2024 / Accepted: 22 August 2024

Abstract
In the context of modern industrialization and global development, blasting operations have become essential for meeting the growing demand for raw materials through large-scale opencast mining. However, if not meticulously planned and executed, blasting can lead to adverse outcomes, including backbreak, flyrock, and structural damage caused by vibrations. These issues can significantly undermine operational safety, reduce efficiency, and negatively impact environmental sustainability. Addressing these challenges requires innovative control techniques, including empirical approaches like vibration analysis, machine learning methods, and numerical simulations, to mitigate the negative impacts effectively. This paper focuses on a numerical approach to controlling backbreak, presenting a comprehensive 3-dimensional finite element (3D FE) model developed to simulate rockmass deformation under blast-load conditions. The model is implemented using Ansys Explicit Dynamics, incorporating the Drucker-Prager strength model and the Jones-Wilkins-Lee equation of state for explosives to accurately predict the extent of rock breakage zones. To evaluate its predictive accuracy, this 3D FE model is compared with 3-dimensional nearfield vibration models. Our findings reveal that the FE model closely aligns with both the vibration model outcomes and field observations, establishing its reliability in predicting backbreak without the need for historical blasting data. This aspect is particularly valuable for preliminary checks in new blasting sites, where historical data may not be available. By offering a dependable alternative for predicting the rock breakage zone extent, the FE model significantly contributes to the refinement of blasting designs, enhancing the safety, productivity, and environmental stewardship of surface mining operations.

Keywords Three-dimensional finite element modeling (3D FE) · Blasting · Rockmass deformation · Backbreak · Three-dimensional nearfield vibration

1 Introduction

Surface mining, distinguished by its extensive mechanization and high productivity, serves as a primary method for extracting minerals, fossil fuels, and metals. The drilling-blasting technique, a predominant strategy for rock fragmentation in open-pit mining, facilitates rock breakage prior to processes such as loading and hauling. Despite the acknowledged efficiency and effectiveness of blasting, its adverse effects—including blast-induced ground vibration, flyrock, air overpressure, air pollution, and backbreak—present considerable challenges [1]. Notably, backbreak critically affects operational safety by potentially causing slope failures, boulder formation, and complicating machinery operations on the bench, thus underlining the importance of accurate backbreak estimation in research efforts.

Blast-induced rock damage zones are broadly categorized into the overbreak and cracked zones. Within the context of surface blasting, the overbreak zone, encompassing backbreak and sidebreak, denotes areas where the rock mass is damaged enough to become excavatable. Conversely, the cracked zone refers to regions where the blast-induced strain either expands existing fractures or initiates new ones, without rendering the rock mass excavatable [2]. A schematic representation illustrating different types of damages associated with surface blasting is depicted in Fig. 1.

✉ Satyabrata Behera
sbehera.min@iitbhu.ac.in

[1] Indian Institute of Technology, BHU, Varanasi, India

[2] Indian Institute of Technology, Kharagpur, India

Published online: 18 September 2024

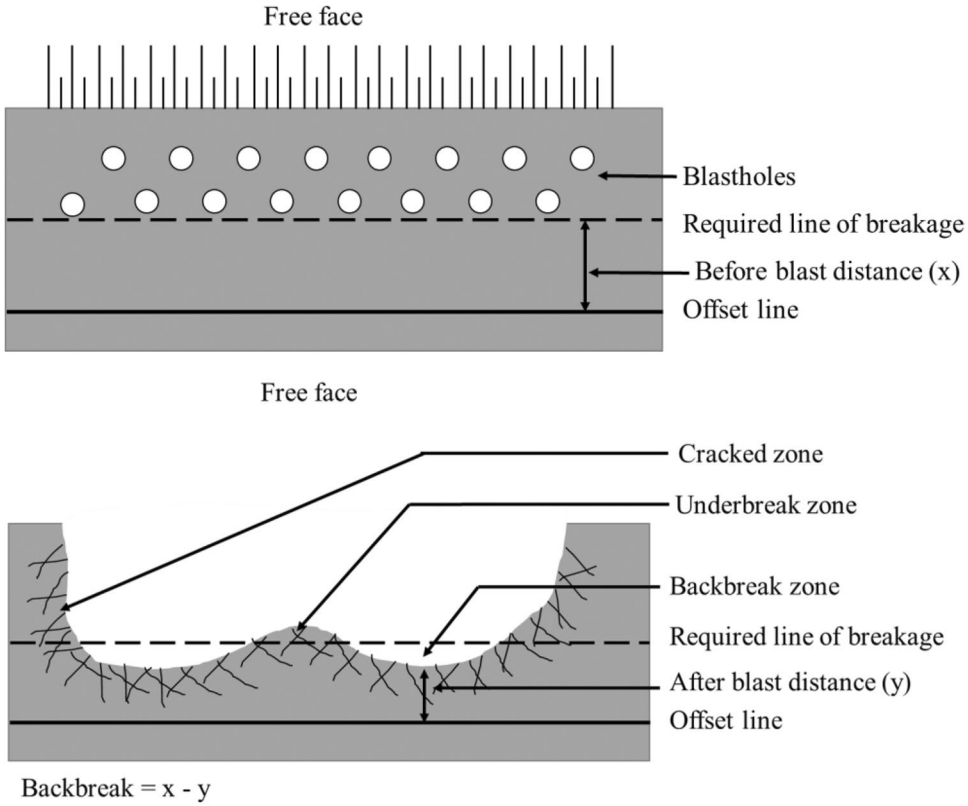

Fig. 1 Schematic representation illustrating different types of damages associated with surface blasting and offset measurement technique

Measurement techniques for these damages vary, tailored to specific geo-mining conditions. Backbreak measurement often involves offset surveying and photographic methods, contrasting the distance between a pre-marked offset line and the post-blast damaged crest line to quantify damage. Evaluating the cracked zone, potentially invisible or below the surface, requires geophysical tools like seismic imaging, borehole cameras, and acoustic and optical borehole wall imaging techniques for detecting fractures within the rock mass [3–11].

Given the complexity of rock damage, researchers have developed predictive models to estimate potential damage before blasting. These models, ranging from vibration-based to statistical and numerical analyses, aim to bolster safety and efficiency in mining operations. Vibration-based models, extensively utilized due to their adaptability across geotechnical conditions, are supported by the contributions of numerous researchers [3, 4, 12–17, 17–39]. Similarly, statistical methods and soft-computing techniques, including neural networks and genetic algorithms, have been explored for forecasting blast performance and mitigating adverse effects [40–50].

Vibration-based prediction models are the most popular type of backbreak prediction models, where blast-induced ground vibrations are measured in peak particle velocity (PPV) expressed in millimeters per second. The threshold level of PPV for rock damage is defined as the PPV level at the boundary of the damaged zone, which is the minimum level at which the rock is damaged. By using this threshold PPV limit, scientists have predicted the extent of blast-induced damage zones. Vibration-based damage predictive models can broadly be classified into three types: (i) extrapolation of far-field measurement, (ii) nearfield measurement, and (iii) nearfield modeling. In the extrapolation of far-field measurement, PPV is measured at a safe distance from the blast hole, and then extrapolated to the damaged length to determine the threshold PPV level for rock damage. Bauer and Calder [13] indicated no fracturing of rock mass when the PPV value is less than 254 mm/s. In the range of 254–635 mm/s, fine tensile slabbing occurs, while 635–2540 mm/s causes strong tensile slabbing, and PPV above 2540 mm/s leads to complete rock mass deformation. Langefors and Kihlstrom [29] proposed that PPV in the range of 305–610 mm/s can result in rock fall in unlined tunnels. Oriard [51] suggested that most rock mass damage occurs at PPV levels above 635 mm/s. Meyer and Dunn [31], studying blast vibrations at the Perseverance Nickel mine in Australia, found the threshold PPV level for rock damage to be 600 mm/s, with minor damage occurring at 300 mm/s. In near-field measurement, the PPV level is measured directly near the blast hole up to the point where damage has resulted, and the threshold PPV level is estimated. Bogdanoff [52] measured blast vibration at distances between 0.25 and 1.0 m outside tunnel perimeter holes, finding the PPV in the damaged zone to be between 2000 and 2500 mm/s. Bhagade and Murthy [3]

measured vibration on a dragline face and suggested a PPV of 344.28 mm/s for a backbreak up to 5.5 m for dragline overburden blasting.

This paper investigates the efficacy of finite element method (FEM)-based numerical models, specifically utilizing Ansys Explicit Dynamics, for simulating specific blasting scenarios without the need for physical experimentation. The focus is on the design and analysis of critical blasting operations within a limestone rock mass. By comparing simulation results with actual blasting experiments and employing a 3D nearfield vibration method for performance analysis, this study aims to validate the reliability of 3D FE simulations in accurately predicting real-world blast outcomes.

This research takes a novel step by incorporating day-to-day production blast rounds into the analysis, thereby bridging the theoretical simulations with practical blasting operations. This integrative approach not only provides a comprehensive understanding of the impacts of routine blasting on rock mass integrity but also showcases the practical applicability of Ansys Explicit Dynamics in optimizing blast designs for enhanced safety and efficiency in the mining industry. Through this innovative methodology, the study contributes significant insights to the advancement of blasting engineering, underscoring the potential of FEM simulations in improving operational outcomes.

2 Methodology

This research adopts a dual-method approach to evaluate and predict backbreak envelopes in blasting operations. It encompasses a 3D nearfield vibration model and finite element (3D FE)–based simulations, leveraging Ansys Explicit Dynamic tools and the Autodyn solver [53]. These methodologies are designed to offer a detailed analysis of blast-induced rock damage.

2.1 3D Nearfield Vibration Model

Developed by Behera and Dey [15], the 3D nearfield vibration model introduces a novel method for estimating nearfield peak particle velocity (PPV) around blast sites. It accurately incorporates the impact of the entire explosive charge column by employing a vector summation of elemental charges, thus enhancing the precision in predicting rock damage. The model is expressed through the following equations in Eq. 1.

Resultant PPV equation:

$$v_r = \sqrt{{v_x}^2 + {v_y}^2 + {v_z}^2} \tag{1}$$

where v_x, v_y, and v_z are component of peak particle velocity along X, Y, and Z coordinate axes respectively, calculated as follows:

$$v_x = kq^{\alpha}\left[\sum_{\tau=1}^{\tau=\eta}\left\{\frac{\delta t}{\left\{R^2 + (Z-(\tau-1)\delta t)^2 + S^2\right\}^{\frac{\beta}{2\alpha}}}\right\}\cos(m)\right]^{\alpha}$$

$$v_y = kq^{\alpha}\left[\sum_{\tau=1}^{\tau=\eta}\left\{\frac{\delta t}{\left\{R^2 + (Z-(\tau-1)\delta t)^2 + S^2\right\}^{\frac{\beta}{2\alpha}}}\right\}\cos(n)\right]^{\alpha}$$

$$v_z = kq^{\alpha}\left[\sum_{\tau=1}^{\tau=\eta}\left\{\frac{\delta t}{\left\{R^2 + (Z-(\tau-1)\delta t)^2 + S^2\right\}^{\frac{\beta}{2\alpha}}}\right\}\cos(p)\right]^{\alpha}$$

In these equations, v_r is the resultant peak particle velocity, and m, n, and p are the angles in degrees made between the direction of propagation "AB" and the X, Y, and Z axes, respectively. Other parameters include linear charge concentration (q), total charge length in hole (h), position of elemental charge from the bottom of the hole (t), elemental charge length (δt), number of segments (η), and distances along the X, Y, and Z axes (R,S,Z). k, α, and β are empirical site constants.

This model is site-specific. To employ it for evaluating the backbreak zone, several blast rounds were monitored, and PPV data were recorded. Empirical site constants k, α, β were derived from the measured PPV and the scaled distance. To determine the threshold PPV level for rock damage, one experimental blast comprising a single blasthole was detonated, and all relevant data were collected. This study included 10 production blast rounds and one experimental blast round. The physical conditions of these blast rounds were replicated in 3D design modeler software for numerical analysis. However, geological discontinuities such as pre-existing cracks, joints, and fractures in the rock mass were not considered in the FE-based numerical simulations.

2.2 3D FE-Based Simulation

Numerical simulations have emerged as a pivotal tool in assessing rockmass damage due to blast loading, significantly bolstered by the strides made in computational power since the mid-1990s. The field has seen contributions from a wide array of researchers, who have all applied numerical techniques to simulate the effects of blasting on rock breakage [54–74].

Bobet [75] have underscored the importance of meticulously selecting input parameters in these simulations, which encompass the geological geometry (like layers, depths, extent, and discontinuities), appropriate boundary conditions, and the behavior of materials (be it elastic, plastic, or

viscoelastic). Such meticulous parameter selection has enabled researchers to accurately simulate blasting scenarios, thereby enriching our understanding and analytical capabilities regarding blast-induced phenomena.

The repertoire of software available for simulating rock blasting is diverse. Hao et al. [61], for instance, leveraged the capabilities of AUTODYN2D, a commercial software, to model stress wave propagation through the rockmass and delineate the damage zone surrounding an underground borehole post-explosion. Park and Jeon [67] utilized the Particle Flow Code (PFC) to explore the optimal distancing between contour holes. Similarly, Ma and An [76] employed LS-DYNA for a numerical assessment of blast-induced rock fractures. These studies exemplify the breadth of computational tools and approaches harnessed to advance our comprehension and management of blasting impacts, underlining the crucial role of FE-based simulations in modern geotechnical engineering and mining practices.

In the present study, a 3D finite element method (FEM) alongside the Ansys Explicit Dynamic tool and Autodyn solver was adopted to simulate blast-induced damage within a rockmass. A simplified geometry is constructed for analysis rather than replicating the complex original field geometry. This approach is exemplified by the general opencast blast design and its corresponding simplified model within the Ansys Explicit Dynamic environment, as illustrated in Fig. 2 and Fig. 3 respectively. The simplified model focuses on a single blast hole positioned on an opencast surface bench, characterized by two free surfaces at the front and top, while the other surfaces are treated as continuity boundaries. This model incorporates key elements of the blast design, including a charge column, a booster charge at the base, and stemming material at the top, thus enabling a manageable yet effective simulation of the blasting process.

Figure 3 reconstructs the field geometry within the Ansys DesignModeler. Part A depicts the rectangular cuboid representing the opencast bench with the blast hole; part B shows the fixed support to this cuboid geometry on four faces, excluding the front and top; part C illustrates the impedance boundary for continuity on four faces; and the final part details the detonation point at the bottom of the charge column in part D.

The subsequent phase in our simulation process involves the assignment of engineering data properties to the constructed geometry. This step is crucial as it dictates the physical behavior of the geometry during numerical simulations, effectively representing it through the application of specific engineering data properties. Historically, a variety of material models and constitutive equations have been leveraged to simulate the phenomena of blast-induced rock fracture and damage. For instance, Ma and An [76] applied the Johnson-Holmquist (J-H) material model within LS-DYNA to study blast-induced rock fractures. Similarly, Wei et al. [72] utilized the Jones-Wilkins-Lee (JWL) equation of state (EOS) for TNT, alongside material type 8 in LS-DYNA, to investigate rock mass damage on a granite rock mass. In another example, Wang et al. [77] employed CONC140 material properties for concrete simulations, whereas Banadaki [78] and Banadaki and Mohanty [54] utilized the Johnson-Holmquist constitutive model for rock mass, coupled with the JWL EOS for PETN. Additionally, Onederra et al. [66] explored blast-induced rock damage using the JWL EOS for TNT, integrated with a generalized Drucker-Prager strength model for the rock mass. These precedents demonstrate the diverse approaches and models used to accurately simulate and understand the impact of blasting on rock integrity.

In the present study, the 3D models are analyzed considering material non-linearity and employing the Drucker-Prager yield criterion. The Drucker-Prager failure criterion is a three-dimensional pressure-dependent model that estimates the stress state at which the rock reaches its ultimate strength [79]. It was established as a generalization of the Mohr–Coulomb criterion. Previous studies by Das and Shen [80], Mitelman and Elmo [65], and others have employed the D-P strength model for sandstone in the numerical simulation of blasting. The Jones-Wilkins-Lee (JWL) equation of state (EOS) developed by Kury et al. [81] and Lee et al. [82] is used for explosives that is available in Ansys Explicit Dynamic. The sand materials are used for stemming available in the Ansys library.

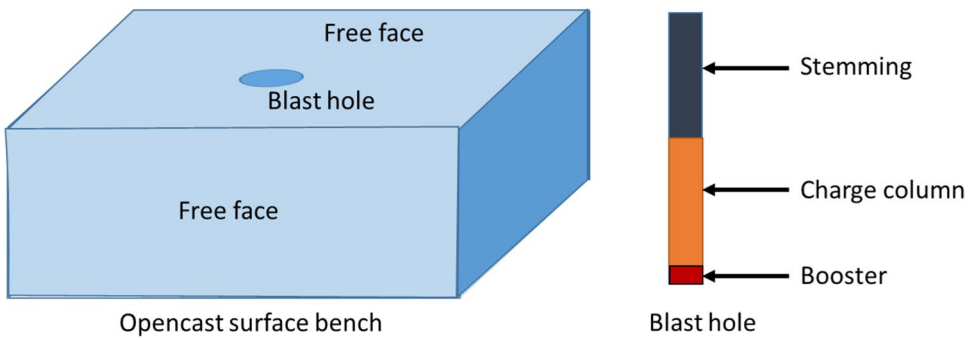

Fig. 2 General opencast working

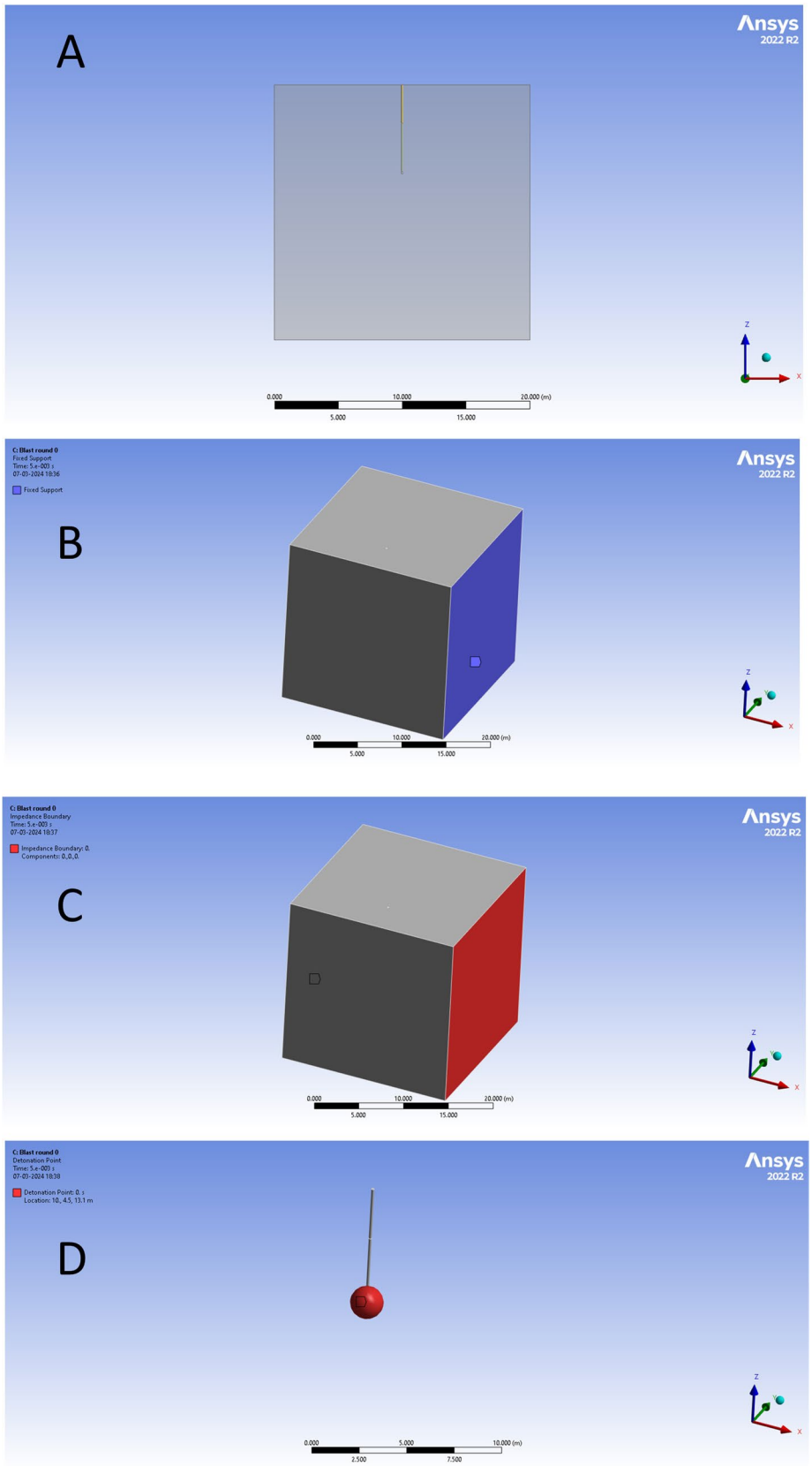

Fig. 3 Geometry design constructed at Ansys Design-Modeler

This section introduces a comprehensive analysis method combining the 3D nearfield vibration model and 3D FE-based simulations to study blast-induced rock damage. Our approach, which merges empirical data with advanced numerical simulations, aims to improve the accuracy and effectiveness of blast designs. By applying these methods, we enhance both our theoretical knowledge and practical skills in mining and construction. The next section will focus on applying this theory in practice, evaluating the models' effectiveness through 10 detailed blast rounds. This transition from theory to real-world application is key to showing the practical advantages of our methodology, with the goal of improving efficiency and safety in blasting operations.

3 Case Study

To study this blast simulation analysis, one experimental blasts and normal production blasts were monitored in the Injepali limestone mine of Karnataka, India. In general, in a regular production blasting, more than one blast holes are blasted in a single round. This study analyzes ten production blast rounds in a limestone rockmass to validate the both 3D nearfield vibration and 3D FE model's applicability in determining the backbreak zone. This mine uses surface mining techniques with a bench height of 10 m. The primary unit operations include drilling, blasting, loading, and transportation. A visual representation of the mine is provided in Fig. 4.

3.1 General Blast Design

The mine adopts a generalized blast pattern to meet its production requirements, depicted in Fig. 5. The pattern incorporates a blasthole with a depth of 5 to10 m and a stemming height of 2.5 to 3.5 m. The blasthole diameter measures 152 mm. The designed burden and spacing fluctuate between 4 and 5 m and 8 to 11 m, respectively. Blasting utilizes Nonel for both down-the-hole and surface connections. A consistent down-the-hole delay of 200 ms is maintained for all holes. The delay between holes is set at 25 ms, while the delay between rows is 67 ms. The rockmass properties specific to the Injepali limestone mine production blasting site are outlined in Table 1, and the explosive charge attributes are detailed in Table 2.

3.2 Monitored Production Blast Rounds

This study scrutinizes one experimental blast and ten production blast rounds to understand the backbreak envelope and verify the accuracy of the 3D nearfield vibration model and 3D FE model in predicting backbreak. A single-hole

Fig. 4 View of the Injepali limestone mine

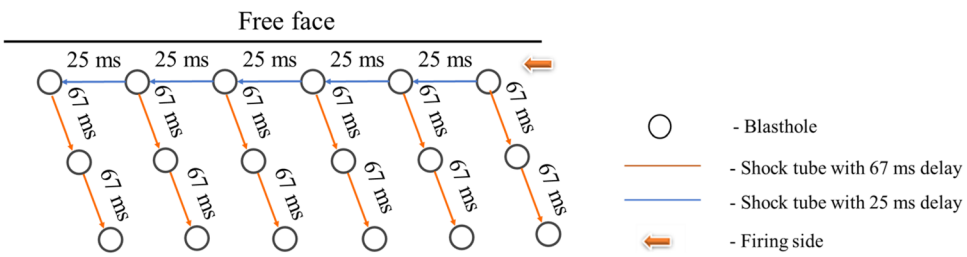

Fig. 5 Generalized blast pattern followed in Injepali limestone mine production blasting with delay arrangement

Table 1 Rockmass properties of the Injepali limestone mine production blasting site

Parameters	Value
Density (kg/m^3)	2552
Young's modulus of elasticity E (GPa)	21.26
UCS (MPa)	76.3
Poisson's ratio	0.12
Internal friction angle ϕ (degree)	43.7
Cohesion (MPa)	16

Table 2 Explosive properties used at Injepali limestone mine production blasting

Parameters	Value
Type of explosive	ANFO
Density (kg/m^3)	820
VOD (m/s)	3500

experimental blast was executed in blast round 0 to estimate the threshold level of PPV for rock mass damage. The specifications for these blast rounds are presented in Table 3. During the blasts, blast-induced ground vibrations were measured using vibration monitoring transducers called geophones. The instrument measures the vibrations through its geophone sensors in terms of peak particle velocity (PPV). The geophones were preferably placed on the same bench at the backside of the last line of the blast holes. Necessary precautions were taken during the installation of the sensors: the sensors were properly levelled, and the arrow indicating the blast direction on the sensor was aligned with the blast. Standard transducers were coupled to the monitoring points, ensuring the surface was compact with no loose material near the geophones, as proper coupling is essential for accurate monitoring; poor coupling can cause the geophone to move independently, leading to distorted results. Ground spikes provided with the standard transducer were used when installing on soft surfaces, and for optimal coupling, transducers were typically buried in the ground. On hard surfaces, especially in hard rock mining conditions, 12-kg sandbags were placed over the transducers to ensure complete coverage. In this research, nearly all positions were on hard surfaces. Following the installation of the geophone sensors, the vibration monitoring instrument recorded specific types of blast-induced ground vibrations. The measured vibration in PPV during the production blasting is given in Table 4. Schematic representation and field observations of the geophone locations during a blast round are given in Fig. 6.

The extent of the visible backbreak is measured by the offset surveying method by taking one baseline offsetting from the last line of the blast hole [6]. This method is the measurement of distance, up to which the backbreak has been occurred. The PPV(v) measured during the blasts were used to establish site-specific constants through regression analysis. Here, the square root scaled distance ($\mathrm{SD} = \frac{\text{Distance between the blast and measuring point } [D]}{\sqrt{\text{Explosive charge per delay } [Q]}}$) is used for regression analysis. The analysis is given in Fig. 7. The mine's blast site-specific parameters are detailed in Table 5. These site-specific constants are the input parameters in the 3D nearfield vibration model. The 3D nearfield vibration model (given in Eq. 1) is utilized to estimate the vibration levels at the boundary of the damaged zone, which is considered as the threshold level of PPV of rock damage for that rockmass. It is defined as the minimum level of PPV at which the rock is damaged.

3.3 Estimation of Threshold Level of PPV

The PPV (peak particle velocity) threshold level is a critical parameter in blasting operations, indicating the minimum PPV at which rock mass begins to experience damage. During the execution of blast round 0, the backbreak distance

Table 3 The blast design specifications of the production blast rounds

Parameters	Values										
Blast round	0	1	2	3	4	5	6	7	8	9	10
Number of holes	01	12	24	22	49	28	40	16	32	32	20
Burden (m)	4.5	5	4	4.5	4	4	4	4.5	4	5	4
Spacing (m)	0	11	10	9	8	8	8	9	8	11	8
Depth (m)	7.0	10.5	7.7	12	6	5	5	5	5	10	7.7
The diameter of the hole (mm)	152	152	152	152	152	152	152	152	152	152	152
Charge length (m)	3.2	6.2	3.8	7.4	2.1	2.5	3	2	1.7	6	3.8
Stemming (m)	3.8	4.3	3.9	4.6	3.9	2.5	2	3	3.3	4	3.9
Charge per hole (kg)	48	93	56	110	32	37.5	44	30	26	90	56
Linear charge density (kg/m)	14.9	14.9	14.9	14.9	14.9	14.9	14.9	14.9	14.9	14.9	14.9
Field observed backbreak (m)	4.6–5.0	6.0–7.0	4.5–5.0	6.5–7.0	4.0–5.0	4.0–5.5	5.5–6.0	4.5–5.5	2.0–5.0	5.0–6.0	5.0–6.0

Table 4 Measured PPV during the production blasting

SL No	Distance (m)	PPV (mm/s)	SL No	Distance (m)	PPV (mm/s)	SL No	Distance (m)	PPV (mm/s)
1	100	44.46	17	110	7.163	33	60	52.14
2	130	24.95	18	125	8.88	34	60	63.73
3	190	9.864	19	125	6.827	35	145	10.48
4	190	10.69	20	140	6.91	36	145	7.79
5	103	68.96	21	90	96	37	180	10.54
6	122	66.45	22	120	65.49	38	180	10.37
7	80	43.88	23	60	65.89	39	100	43.64
8	120	24.369	24	66	62.89	40	100	47.87
9	150	15.44	25	66	50.91	41	100	15.83
10	100	12.18	26	87	32.68	42	130	15.03
11	75	41.55	27	56	43.64	43	38	156.5
12	75	42.6	28	80	31.54	44	38	129.1
13	100	39.9	29	100	17.23	45	60	38.32
14	130	26.22	30	100	16.22	46	60	49.45
15	190	10.34	31	90	21.13	47	115	14.44
16	190	11.1	32	120	10.77	48	115	11.15

was meticulously measured on-site, and the blast round was also analyzed using a 3D nearfield vibration model incorporating site-specific constants. The physical measurement revealed an average backbreak of 4.8 m behind the last line of blast holes. Correspondingly, the nearfield PPV at this distance was calculated using the 3D nearfield vibration model (given in Eq. 1), resulting in a value of 2044 mm/s. This measurement is depicted in Fig. 8, which serves as a visual representation of the damage zone for blast round 0. This PPV level of 2044 mm/s is considered the threshold level for breakage in this particular rock mass.

The blast round 0 was simulated using the Ansys 3D finite element (FE) model, with the results depicted in Fig. 9. The simulation results indicate that the backbreak extends up to 5.5 m from the last blasthole line when a deformation threshold level of 1 mm is considered. This analysis provides an additional perspective on the impact of blasting on the integrity of the rock mass.

Figure 9 presents the total deformation levels simulated by the Ansys 3D FE model, displayed both from a top view along a specific line and in an isometric view to measure the extent of the backbreak. Additionally, the isometric view illustrates the total deformation across the entire rock body for better visualization. In Fig. 9A, a black dot marks the position of a blasthole relative to the free face, with the deformation observed behind this hole representing the backbreak.

Figure 10 shows the relationship between the deformation levels at different points along line 1–2 (as shown in Fig. 9), starting from the free face and extending to the back of the blasthole. An arrow in the Fig. 10 indicates the position of the blasthole, located 4.5 m from the free face on the horizontal axis, while the vertical axis represents the total deformation levels. From the position of the blasthole, the deformation levels gradually decrease. The backbreak distance, defined as the distance from the back of the blasthole to the point where deformation decreases to the 1-mm threshold level, is determined to be 5.5 m.

4 Result

The comparative analysis of backbreak predictions from ten production blast rounds, processed using the 3D nearfield vibration model and the 3D finite element (FE) model, provides significant insights into the predictive accuracy and applicability of both models. For these analyses, only the last line of blast holes was considered, as these holes predominantly influence backbreak (Ibarra et al., 1996; Dey, 2004).

This study employs the 3D nearfield vibration model, as described in Eq. 1, to determine the extent of damage beyond the last row of blast holes. The model accounts for the threshold levels of peak particle velocity (PPV) for rock damage, which were previously established from the single charge column blast in blast round 0.

As shown in Fig. 11, the blast designs for these rounds were configured with delays to ensure that no two holes were detonated simultaneously. The delay number "0" was fired first, followed sequentially by the next higher delay numbers, ensuring independent detonation of each hole at a specific time. Consequently, for the backbreak calculation in the 3D nearfield vibration model, the effect of a single blast hole was considered independently. The same approach was

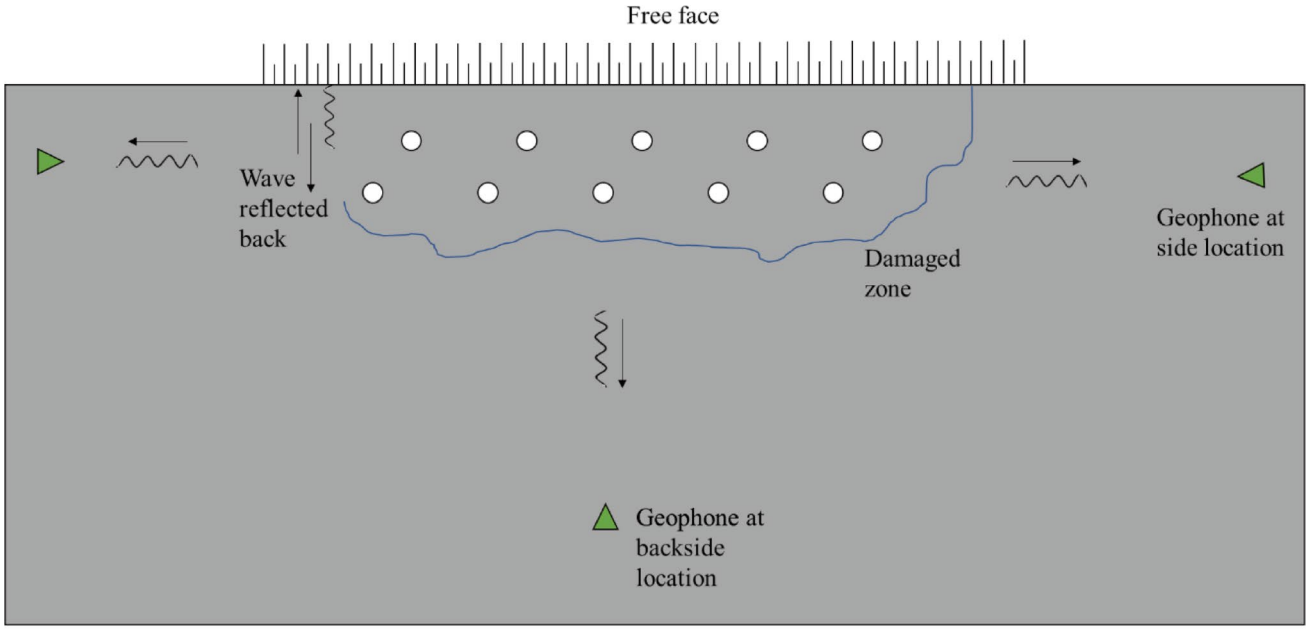

A. Schematic representation

B. Field observation

Fig. 6 Schematic representation and field observations of the geophone locations during a blast round

applied in the Ansys 3D FEM analysis, where only the effect of one blast hole was analyzed.

Each blast round's design, including the analysis of backbreak at the surface by the vibration model, backbreak at the surface by the FE model, and the deformation and backbreak distance as represented by the FE model, is illustrated in Fig. 11. In the blast design, blast holes are indicated by circles, each labelled with its delay number and firing sequence.

A comparative analysis between the 3D nearfield vibration model and the 3D FE model outputs for backbreak is presented in Table 6. The mean absolute percentage deviation analysis results are shown in Table 7, and the box plot of absolute percentage deviations for the 3D nearfield vibration model and the 3D FE model is provided in Fig. 12.

4.1 Backbreak Predictions by the 3D Nearfield Vibration Model

Backbreak predictions at the surface by the 3D nearfield vibration model are depicted through scatter plots, which showcase the wavy form of the damage envelope across each blast round. This wavy pattern is a direct result of the independent detonation sequence of the blast holes, initiated with delay number "0" and proceeding sequentially. The extreme points on the scatter plots delineate the boundary

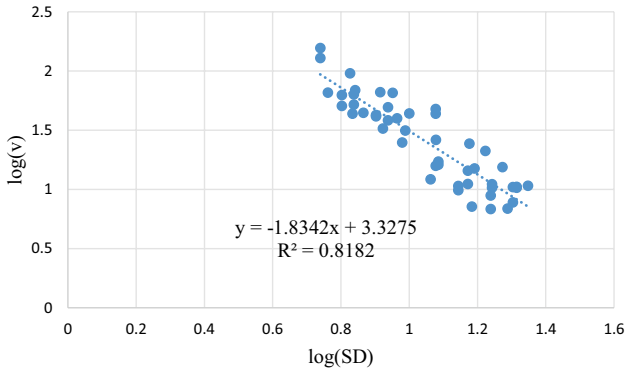

Fig. 7 The vibration predictor equation for Injepali limestone mine production blasting

Table 5 Site-specific parameters of Injepali limestone mine production blasting

Parameter	Value
β	1.834
$\alpha = \beta/2$	0.917
k	2125.6

of the damage envelope, with physical backbreak measurements plotted alongside for comparison.

4.2 Backbreak Predictions by the 3D FE Model

In contrast, the 3D FE model's backbreak predictions are illustrated through top-view diagrams that highlight surface deformation levels with a color gradient ranging from red (high) to blue (low). A scatter plot between deformation level and backbreak distance further elucidates this relationship, with an arrow indicating the blasthole point at one burden distance. The measurements from the blasthole to the 1-mm deformation level provide a quantitative perspective on backbreak predictions by the 3D FE model.

4.3 Comparative Analysis and Implications

The comparative analysis of backbreak predictions from ten production blast rounds, processed using the 3D nearfield vibration model and the 3D finite element (FE) model, provides significant insights into the predictive accuracy and applicability of both models. The deviations in backbreak predictions ranged from 0 to 1.5 m for the 3D nearfield vibration model and from 0.35 to 2.4 m for the 3D FE model, relative to physical measurements. The 3D nearfield vibration model demonstrated a more accurate representation with a smaller range of deviations. This is further supported by the mean absolute percentage deviation (MAPD) analysis, where the 3D nearfield vibration model exhibited a MAPD of 10.08%, compared to 21.34% for the 3D FE model, as shown in Table 7.

When deviations from field observations were examined, the 3D nearfield vibration model showed deviations ranging from – 0.5 to 1.5 m, whereas the 3D FE model exhibited a broader range of deviations from – 1.65 to 2.4 m. This analysis highlights the 3D nearfield vibration model's reliability in predicting backbreak, though it is important to note that this model is more site-specific.

The box plot in Fig. 12 visually represents the spread and variability of these deviations. The plot clearly demonstrates that the 3D nearfield vibration model has a narrower interquartile range, indicating more consistent predictions with fewer extreme deviations. In contrast, the 3D FE model shows a wider interquartile range, reflecting greater variability in its predictions.

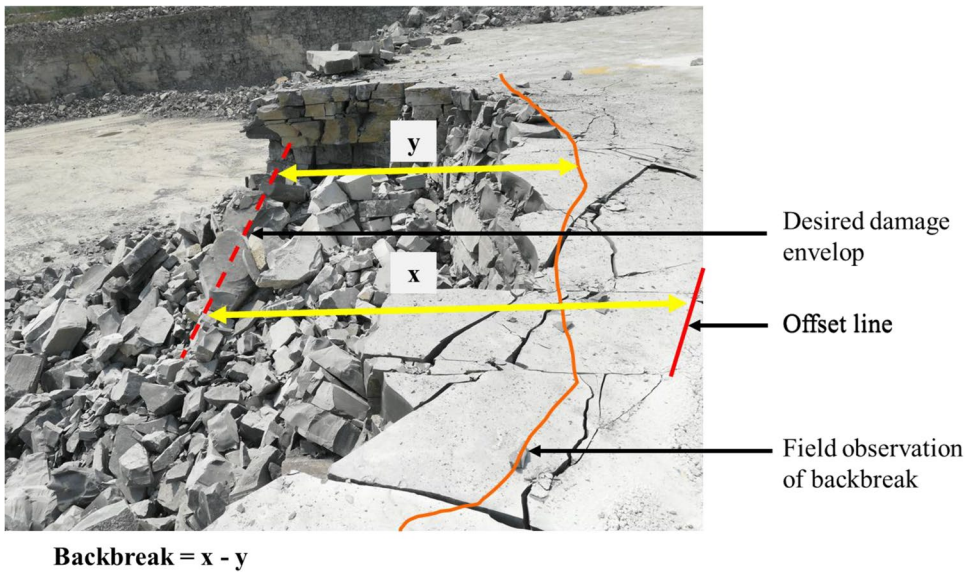

Fig. 8 Damage envelop of blast round 0

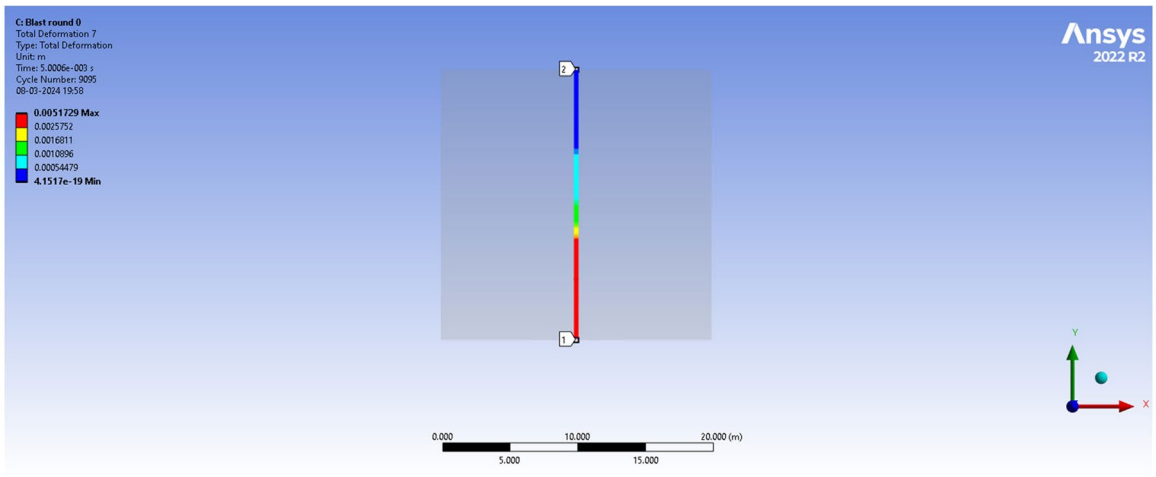

A. Deformation on the particular line 1-2 at the surface Top view.

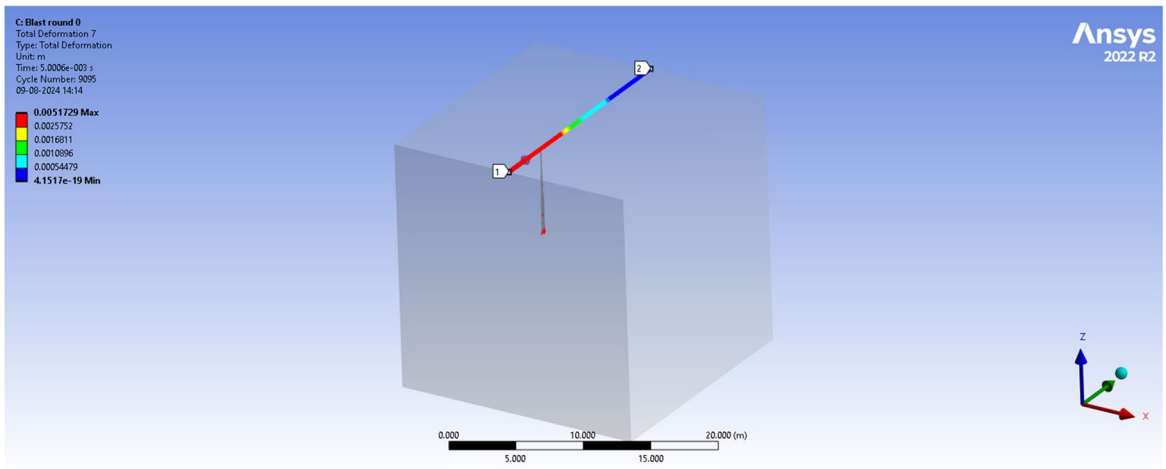

B. Deformation on the particular line 1-2 at the surface Isometric view.

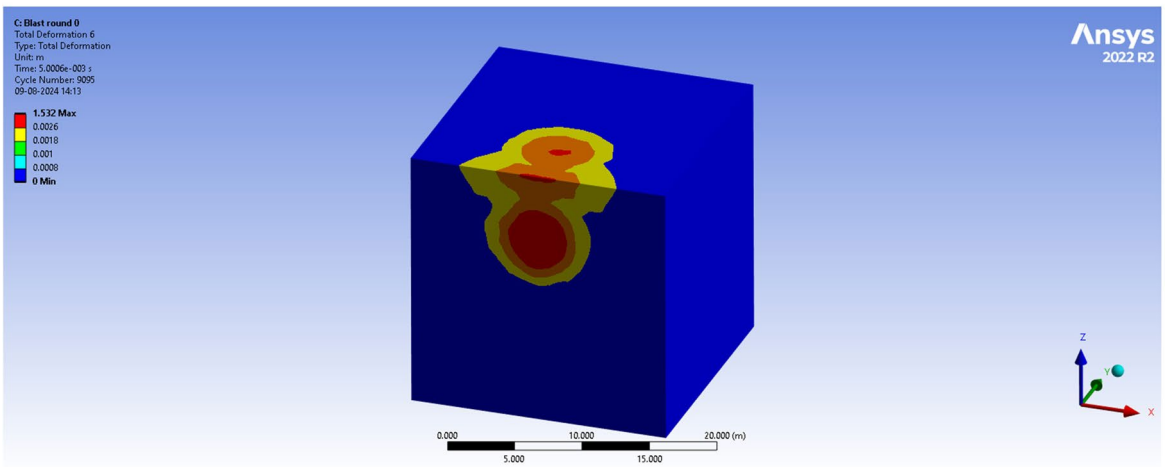

C. Deformation on the whole body Isometric view.

Fig. 9 Backbreak by FE model of blast round 0

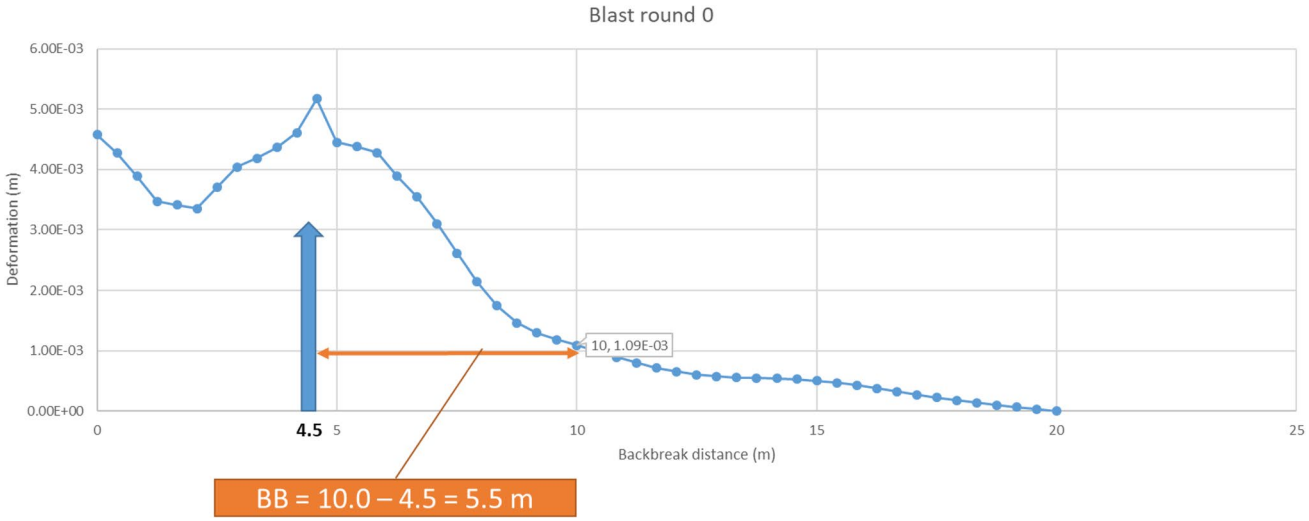

Fig. 10 Deformation level and backbreak distance at the surface graph by FE model

However, the site-specific nature of the 3D nearfield vibration model limits its broader applicability. On the other hand, despite its broader deviation range, the 3D FE model presents a more general approach that is applicable across various blast sites for preliminary backbreak evaluation. Its economic and time-effective nature makes it a viable option for initial surveys in the absence of detailed blast round data.

5 Conclusions

The rockmass excavation industry continues to rely heavily on traditional drilling and blasting methods despite advancements in mechanical cutting technology. This preference is due to the versatility of these methods across varied geo-mining conditions and their cost-effectiveness. However, large-scale production blasting, while efficient, can lead to unintended rockmass damage, particularly in the form of "backbreak." This damage can cause bench instability, create unintended cracks, result in explosive wastage, and lead to suboptimal fragmentation. Addressing these issues can disrupt production schedules, damage equipment, and increase maintenance costs, ultimately reducing productivity. Moreover, blasting in already cracked zones can pose significant risks, such as the occurrence of dangerous flyrocks.

This study presented a comprehensive analysis of backbreak predictions using the 3D nearfield vibration model and the 3D finite element (FE) model across ten production blast rounds. The findings indicate that the 3D nearfield vibration model, with its higher predictive accuracy and deviations ranging from 0 to 1.5 m from physical measurements, offers significant potential for site-specific evaluations. Conversely, the 3D FE model, with deviations ranging from 0.35 to 2.4 m, provides a more general approach to backbreak prediction. Despite its broader deviation range, the 3D FE model's universal applicability and cost-effectiveness make it a practical tool for preliminary backbreak assessments across various blast sites, particularly in scenarios lacking historical blast data.

Both models offer unique contributions to blasting engineering, with the 3D nearfield vibration model excelling in site-specific accuracy and the 3D FE model providing a broader, more versatile application. These complementary tools can be selected based on the specific requirements of the blasting site, the availability of historical data, and the precision needed in backbreak prediction.

Looking forward, integrating these models with emerging technologies such as machine learning and real-time monitoring systems represents a promising avenue for further enhancing predictive accuracy and operational efficiency. Future research could explore the synergistic application of numerical models with empirical and machine learning approaches to develop a holistic predictive framework. Additionally, further investigation into the environmental and societal impacts of blasting operations, including vibration-induced structural damages and air overpressure, is necessary to develop comprehensive mitigation strategies.

In conclusion, the continued advancement of predictive modeling in blasting operations is crucial for achieving safer, more efficient, and environmentally sustainable mining practices. By embracing the insights from this study and exploring innovative technological integrations, the mining industry can navigate the complexities of rock breakage with greater confidence and precision, ushering in a new era of operational excellence.

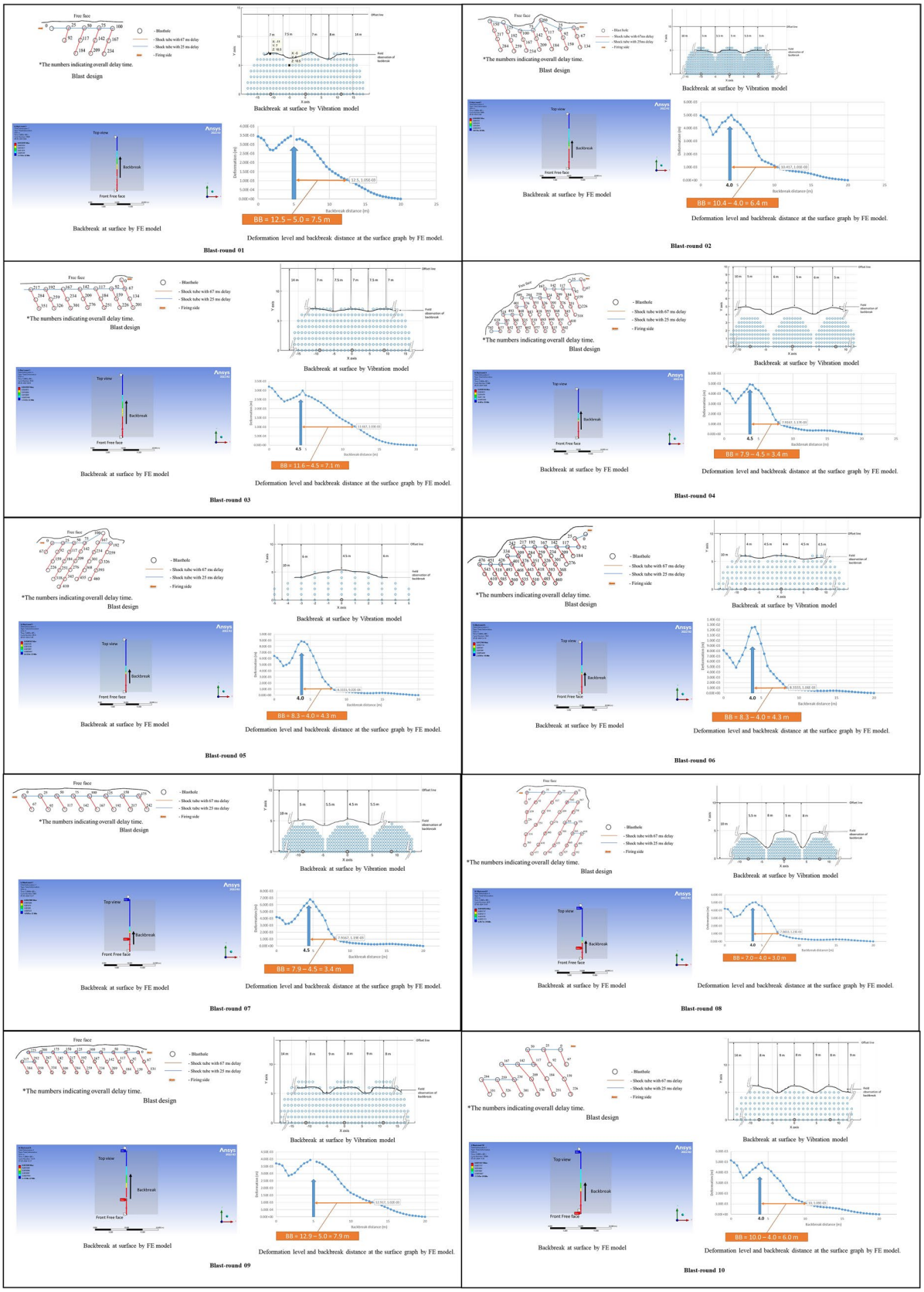

Fig. 11 Backbreak envelop of production blast rounds

Table 6 The comparative analysis of backbreak at production blast rounds

Blast round	Charge length (m)	Backbreak field measurement (m)	PPV by the 3D nearfield vibration model at field observed backbreak point (mm/s)	Backbreak by 3D nearfield vibration model (m)	Backbreak by 3D FE model (m)	3D nearfield vibration model deviation from field measurement (m)	3D FE model deviation from field measurement (m)	Absolute percentage deviation 3D nearfield vibration model (%)	Absolute percentage deviation 3D FE (%)
1	6.2	6.5	2307	7	7.5	0.5	1	7.69	15.38
2	3.8	4.75	2401	5.5	6.4	0.75	1.65	15.79	34.74
3	7.4	6.75	2352	7	7.1	0.25	0.35	3.7	5.19
4	2.1	4.5	1774	3.5	3.4	−1	−1.1	−22.22	−24.44
5	2.5	4.75	2446	5	4.3	0.25	−0.45	5.26	−9.47
6	3	5.75	2210	6	4.3	0.25	−1.45	4.35	−25.22
7	2	5	1799	4.5	3.4	−0.5	−1.6	−10	−32
8	1.7	3.5	2212	3.5	3	0	−0.5	0	−14.29
9	6	5.5	2762	7	7.9	1.5	2.4	27.27	43.64
10	3.8	5.5	2095	5	6	−0.5	0.5	−9.09	9.09

Table 7 Mean absolute percentage deviation analysis results

Parameter	Value
Mean absolute percentage deviation 3D nearfield vibration model (%)	10.082
Mean absolute percentage deviation 3D FE model (%)	21.346
Standard deviation of absolute percentage deviation in 3D nearfield vibration model (%)	8.68246
Standard deviation of absolute percentage deviation in 3D FE model (%)	12.70239

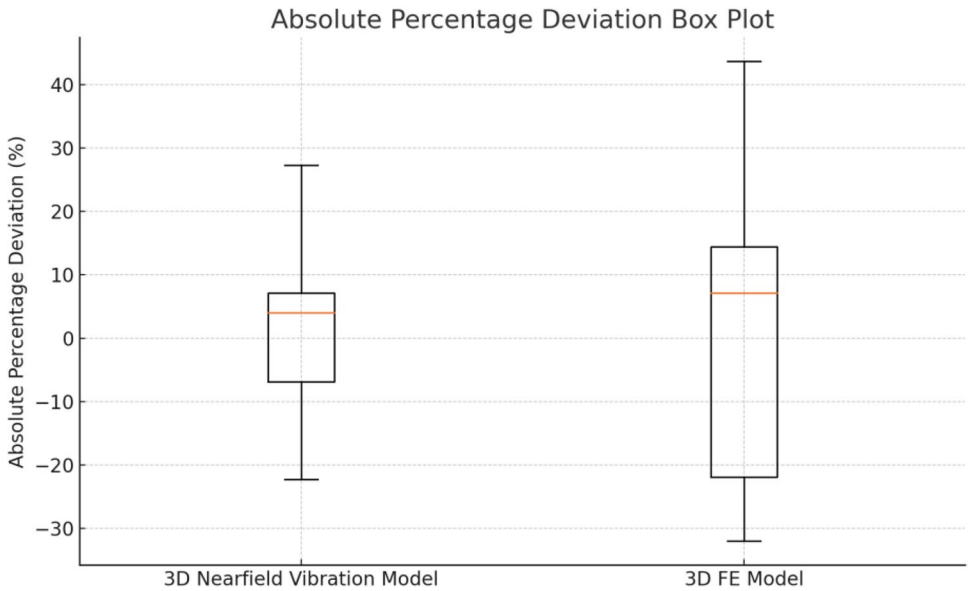

Fig. 12 Box plot of absolute percentage deviations for 3D nearfield vibration model and 3D FE model

Acknowledgements The authors would like to express their sincere gratitude to the Rock Excavation Engineering Lab at the Indian Institute of Technology, Kharagpur, India, the Rock Blasting Lab at the Indian Institute of Technology, BHU, Varanasi, India, and the Injepali Limestone Mine, India, for providing the necessary facilities to carry out this research work. The authors also gratefully acknowledge the use of Ansys® Academic Research Mechanical, Release 2022R2, Help System, for explicit dynamics analysis. This software, provided by ANSYS, Inc., was instrumental in conducting the analyses presented in this study. Without the support and cooperation of these institutions and the use of this critical software, this study would not have been possible. The authors further extend their appreciation to all those who contributed to this research in any capacity.

Data Availability All data, models, or code that support the findings of this study are available in the manuscript.

Declarations

Competing Interest The authors declare that there are no competing interests.

References

1. Sanchidrián JA, Segarra P, López LM (2007) Energy components in rock blasting. Int J Rock Mech Min Sci 44:130–147
2. Rustan AP (1998) Micro-sequential contour blasting—how does it influence the surrounding rock mass? Eng Geol 49:303–313
3. Bhagade NV, Murthy VMSR (2020) Controlling backbreak and enhancing fragmentation in dragline bench blasting—a geo-engineering approach. Arab J Geosci 13:304
4. Dey K, Murthy VMSR (2011) Determining blast damage envelope through vibration model and validation using seismic imaging. Min Technol 120:90–94
5. Mishra D, Chakraborty S, Dey K (2017) Identification of extent of blast-induced crack development using ground penetrating radar (GPR). Allied publisher pvt ltd, New Delhi, pp 349-358
6. Punmia BC, Jain AK, Jain AK (2016) Surveying, vol I, 17th edn. Laxmi Publications
7. Simangunsong GM et al (2004) Field investigation of blast induced damage of the sedimentary strata rock mass at PT Kaltim prime coal, Indonesia. Mater Sci Forum 465–466:175–180
8. Singer JA, Link CA, Iverson SR (2009) High resolution seismic refraction tomography for determining depth of blast induced damage. In: A mine wall. National institute of occupational safety and health, centers for disease control and prevention, order no. 212–2006-M-18282, pp 1–27. Available at: https://stacks.cdc.gov/view/cdc/9899
9. Trivino LF, Mohanty B (2012) Estimation of blast-induced damage through cross-hole seismometry in single-hole blasting experiments. Rock fragmentation by blasting. CRC Press, pp 705-716. https://doi.org/10.1201/b13759-101
10. Williams JH, Johnson CD (2004) Acoustic and optical borehole-wall imaging for fractured-rock aquifer studies. J Appl Geophys 55:151159
11. Yang RL, Rocque P, Katsabanis P, Bawden WF (1994) Measurement and analysis of near-field blast vibration and damage. Geotech Geol Eng 12:169–182
12. Arora S, Dey K (2011) A mathematical model for estimating peak particle velocity in a space between two adjacent blast holes. J Inst Eng (India): Min Eng Div 92(August):3–8
13. Bauer A (1971) Open pit drilling and blasting. J South Afr Inst Min Metall 121(1):115–121
14. Behera S, Dey K (2022) A mathematical model for estimating nearfield peak particle velocity in a 3D space surrounding a blasthole. In rock fragmentation by blasting - Fragblast 13. Metallurgical Industry Press, Beijing, pp 337-346
15. Behera S, Dey K (2022) A PPV-based prediction model to construct damage envelop for crater blasts. J Inst Eng India Ser D 103:13–23
16. Behera S, Dey K (2023) A 3D nearfield vibration model for simultaneous blasting of multiple holes in the sedimentary rock formation. Mater Today Commun 35:106229
17. Blair D, Minchinton A (1997) On the damage zone surrounding a single blasthole. Fragblast 1:59–72
18. Blair DP (2007) A comparison of Heelan and exact solutions for seismic radiation from a short cylindrical charge. Geophysics 72:E33–E41
19. Blair DP (2008) Non-linear superposition models of blast vibration. Int J Rock Mech Min Sci 45:235–247
20. Blair DP (2010) Seismic radiation from an explosive column. Geophysics 75:E55–E65
21. Blair DP (2014) Blast vibration dependence on charge length, velocity of detonation and layered media. Int J Rock Mech Min Sci 65:29–39
22. Dey K, Murthy VMSR (2012) Prediction of blast-induced overbreak from uncontrolled burn-cut blasting in tunnels driven through medium rock class. Tunn Undergr Space Technol 28:49–56
23. Edwards AT, Northwood TD (1960) Experimental studies of the effects of blasting on structures. The Engineer:538–546
24. Gómez S, Sanchidrián JA, Segarra P (2020) Near-field vibration from blasting and rock damage prediction with a full-field solution. Int J Rock Mech Min Sci 134:104357
25. Heelan PA (1953) On the theory of head waves. Geophysics 18:871–893
26. Hustrulid WA (2005) Blasting principles for open pit mining. In: Set of 2 volumes: general design concepts, theoretical foundations, 1st edn. CRC Press
27. Hustrulid WA, Lu WB (2002) Some general concepts regarding the control of blast induced damage during rock slope excavation. In: Wang XG (ed) Proceedings of the 7th international symposium on rock fragmentation by blasting. Metallurgical Industry Press, Beijing, pp 595–604
28. Iverson SR, Kerkering JC, Hustrulid WA (2008) Application of the NIOSH-modified Holmberg-Persson approach to perimeter blast design. In the national institute for occupational safety and health (NIOSH). Mining Publication
29. Langefors U, Kihlstrom B (1973) The modern technique of rock blasting. Wiley, New York
30. Meredith JA (1991) Numerical and analytical modelling of downhole seismic sources--the near and far field. Doctoral thesis, Massachusetts Institute of Technology, Department of Earth, Atmospheric, and Planetary Sciences. http://hdl.handle.net/1721.1/13755
31. Meyer T, Dunn PG (1996) Fragmentation and rock mass damage assessment – sunburst excavator and Drill and blast. In: Proceedings of the NARMS 1996 – rock mechanics tools and techniques, pp 609–617
32. Murthy VMSR, Dey K, Raitani R (2003) Prediction of Overbreak in underground tunnel blasting: a case study. Journal of Canadian Tunneling Canadien 2003:109–115
33. Murthy VMSR, Dey K (2001) Roof damage prediction in solid blasting - an approach. Minetech 25(5/6):43–53
34. Murthy VMSR, Dey K (2003) Predicting overbreak from blast vibration monitoring in a lake tap tunnel–a success story. Fragblast 7:149–166
35. Murthy VMSR, Dey K (2004) Development of predictive models for controlling blast-induced overbreak in tunnels. Journal of Rock Mechanics and Tunneling Technology 10:31–47
36. Oriard LL (1982) Blasting effects and their control. In: Hustrulid (ed) Underground mining methods handbook. Denver, SME of AIME, pp 1590–1603
37. Paurush P, Rai P, Sharma SK (2021) Selection of blasting design parameters affecting peak particle velocity—a case study. Mining Metall Explor 38:1435–1447
38. Persson P-A (1997) The relationship between strain energy, rock damage, fragmentation, and throw in rock blasting. Fragblast 1:99–110
39. Rustan A, Naarttijärvi T, Ludvig B (1985) Controlled blasting in hard intense jointed rock in tunnels. CIM Bull 78:63–68
40. Ebrahimi E, Monjezi M, Khalesi MR, Armaghani DJ (2016) Prediction and optimization of back-break and rock fragmentation using an artificial neural network and a bee colony algorithm. Bull Eng Geol Environ 75:27–36

41. Esmaeili M, Osanloo M, Rashidinejad F, Aghajani Bazzazi A, Taji M (2014) Multiple regression, ANN and ANFIS models for prediction of backbreak in the open pit blasting. Eng Comp 30:549–558
42. Himanshu VK et al (2018) Multivariate statistical analysis approach for prediction of blast-induced ground vibration. Arab J Geosci 11:460
43. Iphar M, Yavuz M, Ak H (2008) Prediction of ground vibrations resulting from the blasting operations in an open-pit mine by adaptive neuro-fuzzy inference system. Environ Geol 56:97–107
44. Khandelwal M, Monjezi M (2013) Prediction of backbreak in open-pit blasting operations using the machine learning method. Rock Mech Rock Eng 46:389–396
45. Mohamadnejad M, Gholami R, Ataei M (2012) Comparison of intelligence science techniques and empirical methods for prediction of blasting vibrations. Tunn Undergr Space Technol 28:238–244
46. Mohammadnejad M, Gholami R, Sereshki F, Jamshidi A (2013) A new methodology to predict backbreak in blasting operation. Int J Rock Mech Min Sci 60:75–81
47. Monjezi M, Amini Khoshalan H, Yazdian Varjani A (2012) Prediction of flyrock and backbreak in open pit blasting operation: a neuro-genetic approach. Arab J Geosci 5:441–448
48. Monjezi M, Rizi SMH, Majd VJ, Khandelwal M (2014) Artificial neural network as a tool for backbreak prediction. Geotech Geol Eng 32:21–30
49. Monjezi M, Dehghani H (2008) Evaluation of effect of blasting pattern parameters on back break using neural networks. Int J Rock Mech Min Sci 45:1446–1453
50. Sharma M, Agrawal H, Choudhary BS (2022) Multivariate regression and genetic programming for prediction of backbreak in open-pit blasting. Neural Comput & Applic 34:2103–2114
51. Oriard LL (1972) Blasting effects and their control in open pit mining. In: Proceedings of the second international conference on stability in open pit mining. AIME, Vancouver, pp 197–222
52. Bogdanoff I (1993) Vibration measurements in the damage zone in tunnel blasting. In: Rock fragmentation by blasting, 1st edn. CRC Press
53. ANSYS, Inc. (2022) Ansys® academic research mechanical, release 2022R2, help system, explicit dynamics. Retrieved from https://www.ansys.com on December 2023
54. Banadaki MMD, Mohanty B (2012) Numerical simulation of stress wave induced fractures in rock. Int J Impact Eng 40–41:16–25
55. Donzé F, Magnier S-A, Bouchez J (1996) Numerical modeling of a highly explosive source in an elastic-brittle rock mass. J Geophys Res B: Solid Earth 101:3103–3112
56. Donzé F, Magnier S-A (1995) Formulation of a 3-D numerical model of brittle behavior. Geophys J Int 122:790–802
57. Donze FV, Bouchez J, Magnier SA (1997) Modeling fractures in rock blasting. Int J Rock Mech Mining Sci Geomech Abstracts 34:1153–1163
58. Fakhimi A, Lanari M (2014) DEM–SPH simulation of rock blasting. Comput Geotech 55:158–164
59. Grady DE, Kipp ME (1980) Continuum modeling of explosive fracture in oil shale. Int J Rock Mech Mining Sci Geomech Abstracts 17:147–157
60. Grady DE, Kipp ME (1987) 10 - Dynamic rock fragmentation. In fracture mechanics of rock (ed. Atkinson BK. Academic Press, London, pp 429-475. https://doi.org/10.1016/B978-0-12-066266-1.50015-6
61. Hao H, Ma G, Zhou Y (1998) Numerical simulation of underground explosions. Fragblast 2:383–395
62. Holmquist TJ, Templeton DW, Bishnoi KD (2001) Constitutive modeling of aluminum nitride for large strain, high-strain rate, and high-pressure applications. Int J Impact Eng 25:211–231
63. Liu L, Katsabanis PD (1997) Development of a continuum damage model for blasting analysis. Int J Rock Mech Min Sci 34:217–231
64. Lu Y, Xu K (2004) Modeling of dynamic behavior of concrete materials under blast loading. Int J Solids Struct 41:131–143
65. Mitelman A, Elmo D (2014) Modeling of blast-induced damage in tunnels using a hybrid finite-discrete numerical approach. J Rock Mech Geotech Eng 6:565–573
66. Onederra IA, Furtney JK, Sellers E, Iverson S (2013) Modeling blast induced damage from a fully coupled explosive charge. Int J Rock Mech Min Sci 58:73–84
67. Park B, Jeon S (2005) Characteristics of blast-induced fracturing for the determination of optimal spacing in contour blasting using bonded particle model. Geosyst Eng 8:15–23
68. Potyondy DO, Cundall PA (2004) A bonded-particle model for rock. Int J Rock Mech Min Sci 41:1329–1364
69. Taylor LM, Chen E-P, Kuszmaul JS (1986) Microcrack-induced damage accumulation in brittle rock under dynamic loading. Comput Methods Appl Mech Eng 55:301–320
70. Vishwakarma AK, Himanshu VK, Dey K (2024) Evaluation of optimum burden for the excavation of narrow vein ore deposits using numerical simulation. Rock Mech Rock Eng 57:945–960
71. Wang J, Yin Y, Esmaieli K (2018) Numerical simulations of rock blasting damage based on laboratory-scale experiments. J Geophys Eng 15:2399–2417
72. Wei XY, Zhao ZY, Gu J (2009) Numerical simulations of rock mass damage induced by underground explosion. Int J Rock Mech Min Sci 46:1206–1213
73. Yi C, Sjöberg J, Johansson D (2017) Numerical modeling for blast-induced fragmentation in sublevel caving mines. Tunn Undergr Space Technol 68:167–173
74. Zhang Z, Gao W, Li K, Li B (2020) Numerical simulation of rock mass blasting using particle flow code and particle expansion loading algorithm. Simul Model Pract Theory 104:102119
75. Bobet A (2000) The initiation of secondary cracks in compression. Eng Fract Mech 66:187–219
76. Ma GW, An XM (2008) Numerical simulation of blasting-induced rock fractures. Int J Rock Mech Min Sci 45:966–975
77. Wang Y, Zhu Z, Zhou Z, Xie H (2009) Numerical investigation of blasting-induced damage in concrete slabs. In: Yuan Y, Cui J, Mang HA (eds) Computational structural engineering. Springer, Dordrecht, pp 569–574. https://doi.org/10.1007/978-90-481-2822-8_72
78. Banadaki MMD (2011) Stress-wave induced fracture in rock due to explosive action (doctoral thesis, University of Toronto). University of Toronto Libraries. https://hdl.handle.net/1807/27567
79. Deb D (2012) Finite element methods: concepts and applications in Geomechanics, 2nd edn. PHI
80. Das S, Shen L (2014) Experimental and numerical investigation of dynamic failure of sandstone under high strain rates. In: 23rd Australasian conference on the mechanics of structures and materials (ACMSM23), vol 2
81. Kury JW et al (1965) Metal acceleration by chemical explosives. In: Fourth detonation symposium, pp 3–13
82. Lee EL, Horning HC, Kury JW (1968) Adiabatic expansion of high explosive detonation products. Lawrence radiation laboratory, University of California, Livermore. TID-4500, UC-4, Chemistry